WELDING RESEARCH

SUPPLEMENT TO THE *WELDING JOURNAL*, FEBRUARY 2024
Sponsored by the American Welding Society

Keyhole Welding with Hybrid Plasma-Free Arc Source

A new method for improving keyhole welding stability was explored

BY Z. LIU, F. LIU, AND J. QIU

Abstract

Improving the keyhole welding process window is challenging work because the force and thermal state in the weld pool are hard to control. A hybrid plasma-free arc source was developed based on a plasma arc torch, sided tungsten was added close to the constraint orifice to form a free arc, and hybrid arcs formed after the free arc was fully absorbed into the constraint arc. In such a one-anode, two-cathode hybrid arc system, the added free arc acts in an assistant role to adjust arc heat output without influencing the arc pressure peak, and the constraint arc acts as the guiding arc to control the arc pressure and slightly incline to the free arc side. Bead-on welding experiments were done to test keyhole welding process behavior with the hybrid arc source, including arc column, keyhole state, weld surface performance, and melting state in the weld pool. Results showed that (1) the hybrid arc can enlarge the stable keyhole welding process window in aspects of welding current and welding speed, and a more-obvious improving effect is obtained with the leading-sided tungsten; (2) the hybrid arc with the rear-sided tungsten has a smooth front weld surface; (3) the increased heat will enlarge the weld cross-section area with no obvious influence to the backside weld width; and (4) the leading keyhole wall is related to the outer tungsten position. The research gives a new method for improving keyhole welding stability.

Keywords

- Hybrid Arc Heat Source
- Keyhole Welding
- Plasma Arc Welding
- Keyhole Stability

https://doi.org/10.29391/2024/103.004

Introduction

Plasma arc welding (PAW) is a highly efficient welding process. It has been applied in the fields of rocket motors (Ref. 1), space shuttle tanks (Ref. 2), and steel structures (Ref. 3). In plasma arc welding, the arc column is highly constrained after it flows through a water-cooled nozzle. The arc performance, including current density, arc pressure, and heat density, is much enhanced over the free arc heat source. The keyhole mode welding process easily forms in a mid-thickness workpiece. When the welding current is high enough, the workpiece will be fully penetrated with an open keyhole growing from the torch side to the workpiece bottom. Keyhole stability is easily disturbed because the gas-liquid interface in the keyhole channel is sensitive to many factors, such as the physical properties of the metal to be welded and the coupling state between the arc jet and weld pool. Keyhole stability is key to getting a stable welding process because the process window is narrow.

Many efforts have been mode to improve the keyhole welding process window in aspects of current waveform and arc performance modification. In a constant parameter welding process, the welding current should be high enough to create powerful arc pressure and hot enough to sustain an open keyhole (Ref. 4). Because the ratio of pressure/current is very high in a plasma arc, slightly increasing or decreasing the welding current will influence the thermal and force balance in the weld pool. Keyhole stability is hard to control. Pulse waveform current was introduced by Zhang to control the keyhole's opening and closing dynamic (Refs. 5, 6). During the peak current stage, powerful arc pressure and heat enlarged the weld pool and opened the keyhole. During the background current stage, low-level heat and pressure were deposited to cool down the weld pool with a closed keyhole. The keyhole opened and closed one time during one pulse period, and a fully penetrated weld was obtained without weld pool collapse. The average welding current was reduced compared with that in the constant-parameters process. Further work to modify the square waveform with a slow-falling edge was done by Zhang's team (Ref. 7) and Wu's team (Ref. 8). The open keyhole was controlled

Table 1 — Keyhole Penetration State				
105 A/0A	**105 A/L40A**	**105 A/L80A**	**105 A/R40A**	**105 A/R80A**
None-penetrated	Unstable penetrated	Stable penetrated	None-penetrated	None-penetrated
110A/0A	110A/L40A	110A/L80A	110A/R40A	110A/R80A
Unstable penetrated	Stable penetrated	Stable penetrated	Unstable penetrated	Stable penetrated
120A/0A	120A/L40A	120A/L80A	120A/R40A	120A/R80A
Stable penetrated	Stable penetrated	Stable penetrated	Stable penetrated	Stable penetrated

to gradually narrow following the welding current; the keyhole behaved smoothly. Arc performance modification was done by adjusting the torch structure. NASA developed a ternary gas plasma arc torch (Ref. 9) in which secondary inert plasma gas flowed through the tubular tungsten, a straighter and stable plasma arc formed, and penetration ability was enhanced. Radial flowing focusing gas was added through the pinhole system in the orifice wall (Ref. 10) or below the orifice (Refs. 11, 12) to further compress the arc jet. Enhancing the penetration ability can reduce the threshold welding current to open a keyhole, but the ratio of pressure/current is increased. To avoid harsh arc pressure damaging the aluminum weld pool in the horizontal position, two pinholes were added aside to the orifice (Ref. 13), and soft PAW was developed. The keyhole weld pool was stabilized under such a soft plasma arc, and high-quality welds were achieved in 8 mm- (0.315 in.-) thick plates (Ref. 14). Hybrid heat source systems based on plasma arc were developed; for example, laser-assisted plasma arc welding (Refs. 15, 16), a PAW-gas metal arc welding (GMAW) hybrid welding process (Refs. 17, 18), and ultrasonic vibration-assisted PAW (Refs. 19, 20). In both hybrid welding processes, welding efficiency and weld quality were improved. In the author's team, a tungsten rod was positioned close to the orifice, and a free arc rooting to the tungsten end was absorbed into the constraint arc and formed a hybrid arc (Ref. 21). The plasma arc acted as the major arc to control the arc pressure and heat in the hybrid arc. The added free arc acted in an assistant role; it had little effect on pressure peak value. That is, in the developed hybrid arc system, the arc heat could be adjusted without changing the arc pressure peak. The sided free arc attracts the major arc to incline to the outer tungsten side; the distribution of arc pressure and heat differ from the original constraint arc, which should affect the keyhole welding process.

In this paper, keyhole welding experiments were carried out to evaluate the effects of hybrid arc direction on the welding process and weld performance. The torch setup and experimental system were first introduced. Arc behaviors, keyhole state, weld surface, and melting state in the weld were presented with varying welding directions and free arc current. Welding speed was also tested.

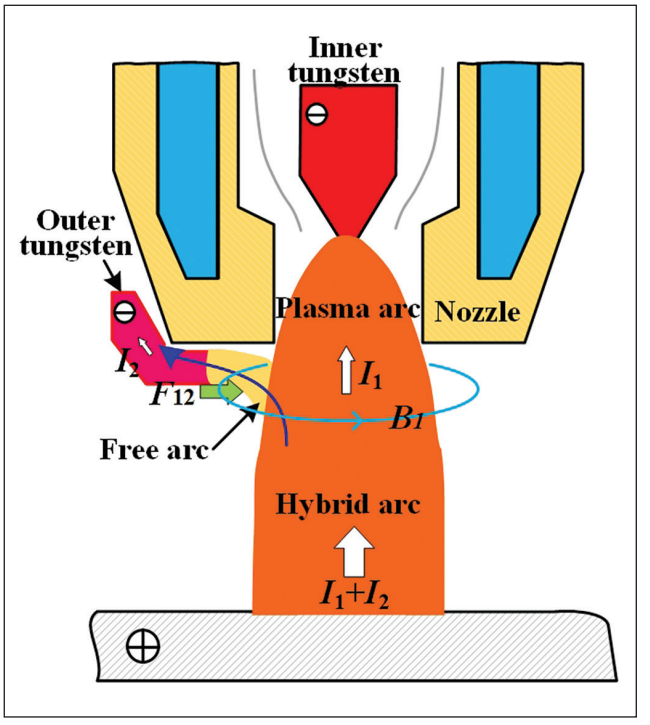

Fig.1 — Hybrid arc principle.

Torch Setup and Welding System

The hybrid plasma-free arc generation principle is schematically shown in Fig. 1. An outer tungsten rod was equipped below the water-cooled orifice in an ordinary PAW torch and connected to the negative terminal of an additional constant current (CC) mode welding power source. The inner tungsten rod formed a plasma arc, while the outer tungsten rod formed a free arc. The two arcs converged into a hybrid arc by Lorentz force. In the arc system, welding current flowed out from the anode workpiece into the hybrid arc and then separated into a constraint arc into the inner tungsten through the orifice (I_1) and a free arc into the outer tungsten (I_2). The heat deposited to the weld pool was controlled with two roads of arc current, while arc pressure was highly related to the constraint arc parameters, including the welding current (I_1) and orifice diameter. The free arc welding current (I_2) had little effect on

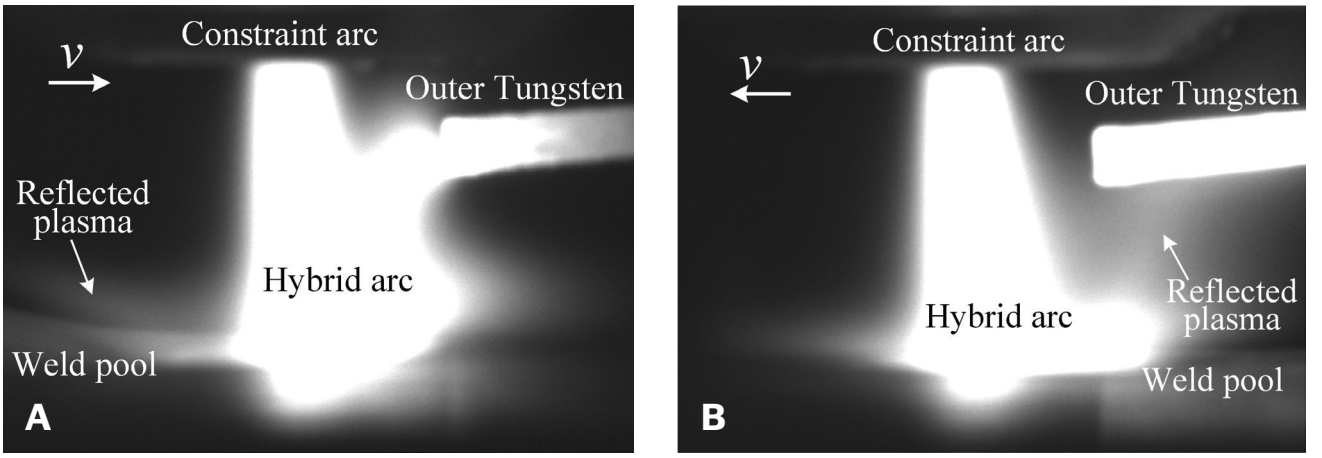

Fig. 2 — Arc behavior: A — Leading sided (120 A/L80 A); B — rear-sided (120 A/R80 A).

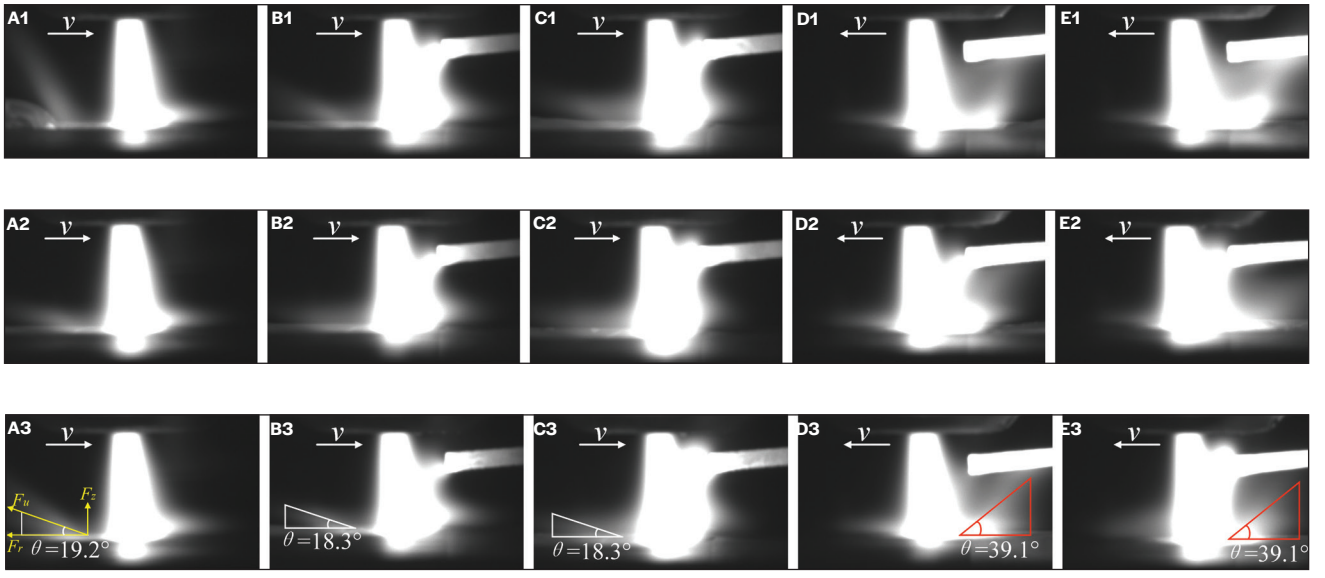

Fig. 3 — Arc behavior: A1 — 105 A/0 A; B1 — 105 A/L40 A; C1 —105 A/L80 A; D1 — 105 A/R40 A; E — 105 A/R80 A; A2 — 110 A/0 A; B2 — 110 A/L40 A; C2 — 110 A/L80 A; D2 — 110 A/R40 A; E2 — 110 A/R80 A; A3 — 120 A/0 A; B3 — 120 A/L40 A; C3 — 120 A/L80 A; D3 — 120 A/R40 A; E3 — 120 A/R80 A.

the arc pressure. In the proposed hybrid arc system, the arc pressure and the arc heat can be decoupling controlled in the system (Ref. 21). Such a bypass arc system works similarly to the consumable double-electrode GMAW system (Ref. 22), where current flows through the wire and is bypassed with a sided arc. In this way, the large wire current creates more heat to melt the wire as well as enough force to detach the droplet, and less heat is deposited into the workpiece. It also works like the arcing wire gas tungsten arc welding system (Ref. 23); the arcing wire current is used to melt the wire without increasing heat into the workpiece.

After the outer tungsten rod is positioned in the bottom of the PAW torch, the free arc attracts the constraint arc inclines to the outer tungsten side. The distribution of arc pressure and arc heat in the hybrid arc differs from those in the single constraint arc. As displayed in Fig. 2, if the outer tungsten tip is positioned ahead (marked as L) to the welding torch, the hybrid arc forward-inclines, while if the outer tungsten tip is posited trailing to the welding torch (marked as R), the hybrid arc rearward-inclines. The solid region in the leading region of the weld pool will experience additional heat and arc pressure when the outer tungsten is positioned on the leading side, and if the tungsten is rear-sided, the liquid weld pool will experience the effect of the free arc. What will happen during the welding process and what welds will be obtained in the two different tungsten positions should be experimentally figured out.

In the plasma arc torch, the water-cooled nozzle has an orifice diameter of 2.8 mm (0.110 in.), and the inner tungsten rod WL20 has a diameter of 4.8 mm (0.189 in.), a tip angle of 45 deg, and setbacks 3 mm (0.118) from the nozzle bottom surface. The outer tungsten rod tip has 2.5 mm (0.098 in.) to the nozzle bottom and 2.5 mm to the torch axis. The nozzle bottom offsets 7 mm (0.275 in.) to the workpiece surface. The plasma gas flow around the inner tungsten is pure argon with a flow rate of 3.0 L (0.792 gal)/min, and the shielding

gas is pure argon with a flow rate of 15 L (3.962 gal)/min. The torch travels at 2.5 mm/s in every test case. The workpieces were SUS304 stainless steel plates with dimensions of 200 mm (7.874 in.) × 60 mm (2.362 in.) × 6 mm (0.236 in.).

In the data acquisition system, two CMOS cameras were used. One was sided to the torch to observe the arc column state. The view direction was vertical to the torch axis and the traveling direction. Another camera was positioned under the workpiece to observe keyhole exit behavior; the camera was equipped with an inclined angle of 70 deg toward the weld pool, as in Ref. 24. During the welding process, the torch and the two cameras were stationary, and while the workpiece traveled at the welding speed, the arc column and keyhole behaviors could hence be captured during the whole welding process.

Two groups of welding processes were carried out with a hybrid arc torch. Test Group 1 used three levels of constraint arc current, 105 A, 110 A, and 120 A, to create different penetration state keyhole weld pools. Two levels of free arc current, 40 A and 80 A, were used with leading-sided or rear-sided positions to observe arc behavior, keyhole penetration state, and weld formation. Test Group 2 used a fixed arc current set – 120 A, 80 A – to test the welding speed window to achieve a stable keyhole welding process.

Results and Discussion

Arc Behavior

Figure 3 and Table 1 present the influence of the free arc and its direction on the penetration state. When the constraint arc current was 105 A, a stiff constraint arc stuck into the weld pool, and the heat and pressure formed in a single arc was not enough to form a fully penetrated keyhole. The plasma gas sprung out through the keyhole entrance to form a clear reflected plasma arc over the weld pool. When a leading-sided free arc was added, it fully absorbed into the plasma arc, the keyhole state transfered from non-penetrated to unstable penetrated at current I_2 of 40 A, and the reflected plasma arc decreased its angle and turned less dense, as shown in Fig. 3B1. If the leading free arc current increased to 80 A, a stable, fully penetrated keyhole formed, and the reflected plasma arc further decreased the angle, as shown in Fig. 3C1. If the free arc was rear-sided, the coupling state between the plasma arc and free arc differed. The free arc did not emit from the outer tungsten tip but was guided by the reflected plasma arc to bridge the tungsten middle and the weld pool. Arc images Figs. 3D1 and 3E1 show that the free arc was not fully absorbed into the plasma arc and the keyhole stayed in a non-penetrated state in the two cases.

As the plasma arc current increased to 110 A, as shown in Fig. 3A2, the heat and pressure formed in a single arc were high enough to form an unstable penetrated keyhole, and the reflected plasma arc over the weld pool was weaker and had a smaller reflected angle compared with that of 105 A (Fig. 3A1). When a leading-sided free arc was added, a stable penetrated keyhole welding process formed at current I_2 of 40 A and 80 A, the free arc was fully absorbed into the plasma arc to form a stable hybrid arc in the two cases, and the reflected plasma arc decreased its angle or even disappeared (Fig. 3C2). When a rear-sided free arc was added, the keyhole state stayed at unstable penetration at current I_2 of 40 A and transfered to a stable penetrated keyhole at current I_2 of 80 A. As shown in arc image Fig. 3D2, the free arc had two paths in the unstable keyhole welding state at I_2 of 40 A: One bridged the outer tungsten tip to the plasma arc to form a hybrid arc, and another was guided by the reflected plasma arc to bridge the outer tungsten middle and the weld pool. At current I_2 of 80 A, as shown in Fig. 3E2, the reflected plasma arc's height was too low to reach the outer tungsten, the free arc was emitted from the tungsten tip and fully absorbed into the plasma arc, as did Fig. 3C2.

The weld surface performances obtained in the cases of current I_2 of 120 A are shown in Fig. 4. Stable fully penetrated welds were achieved in these keyhole welding processes. Every backside weld presented a uniform melting state throughout the whole welding process. In the front surfaces, undercut phenomena were easily found in 120 A/0 A, 120 A/L40 A, and 120 A/L80 A, and the intensity was heaviest in 120 A/0 A and smallest in 120 A/L80 A. In the rear-sided cases, the front surfaces were very smooth.

Table 2 — Process Parameters and Keyhole State in Test Group 2

Test No.	I_1(A)	I_2(A)	ν(mm/s)	Keyhole State
2-1-1	120	0	3.0	Stable open
2-1-2			3.25	Closed
2-2-1	120	L80	3.0	Stable open
2-2-2			3.25	Stable open
2-2-3			3.5	Stable open
2-2-4			3.75	Closed
2-3-1	120	R80	3.0	Stable open
2-3-2			3.25	Stable open
2-3-3			3.5	Unstable open
2-3-4			3.75	Closed

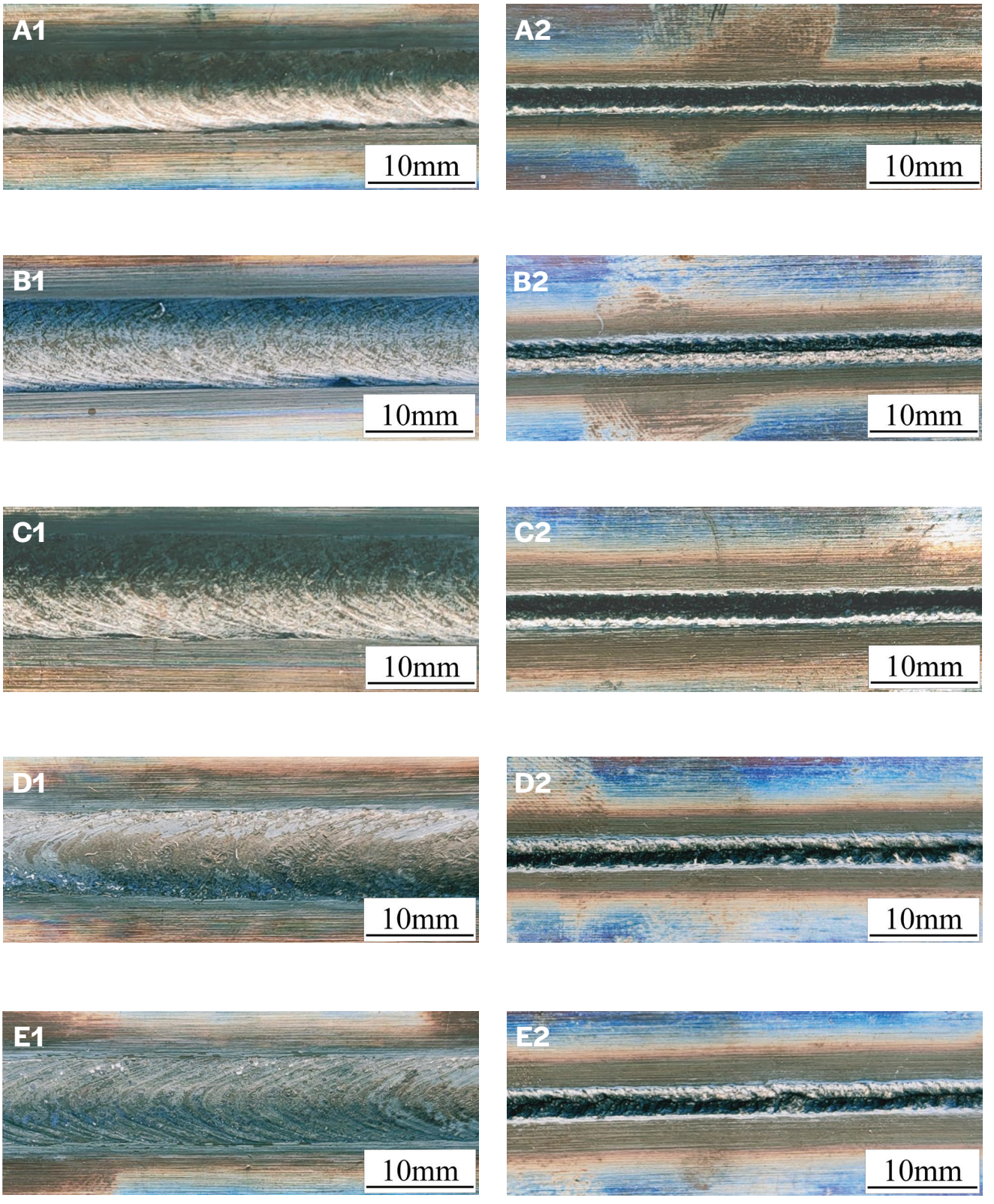

Fig. 4 — Weld surfaces (current I_1 = 120 A): A1 — Front surface (120 A/0 A); A2 — back surface (120 A/0 A); B1 — front surface (120 A/L40 A); B2 — back surface (120 A/L40 A); C1 — front surface (120 A/L80 A); C2 — back surface (120 A/L80 A); D1 — front surface (120 A/R40 A); D2 — back surface (120 A/R40 A); E1 — front surface (120 A/R80 A); E2 — back surface (120 A/R80 A).

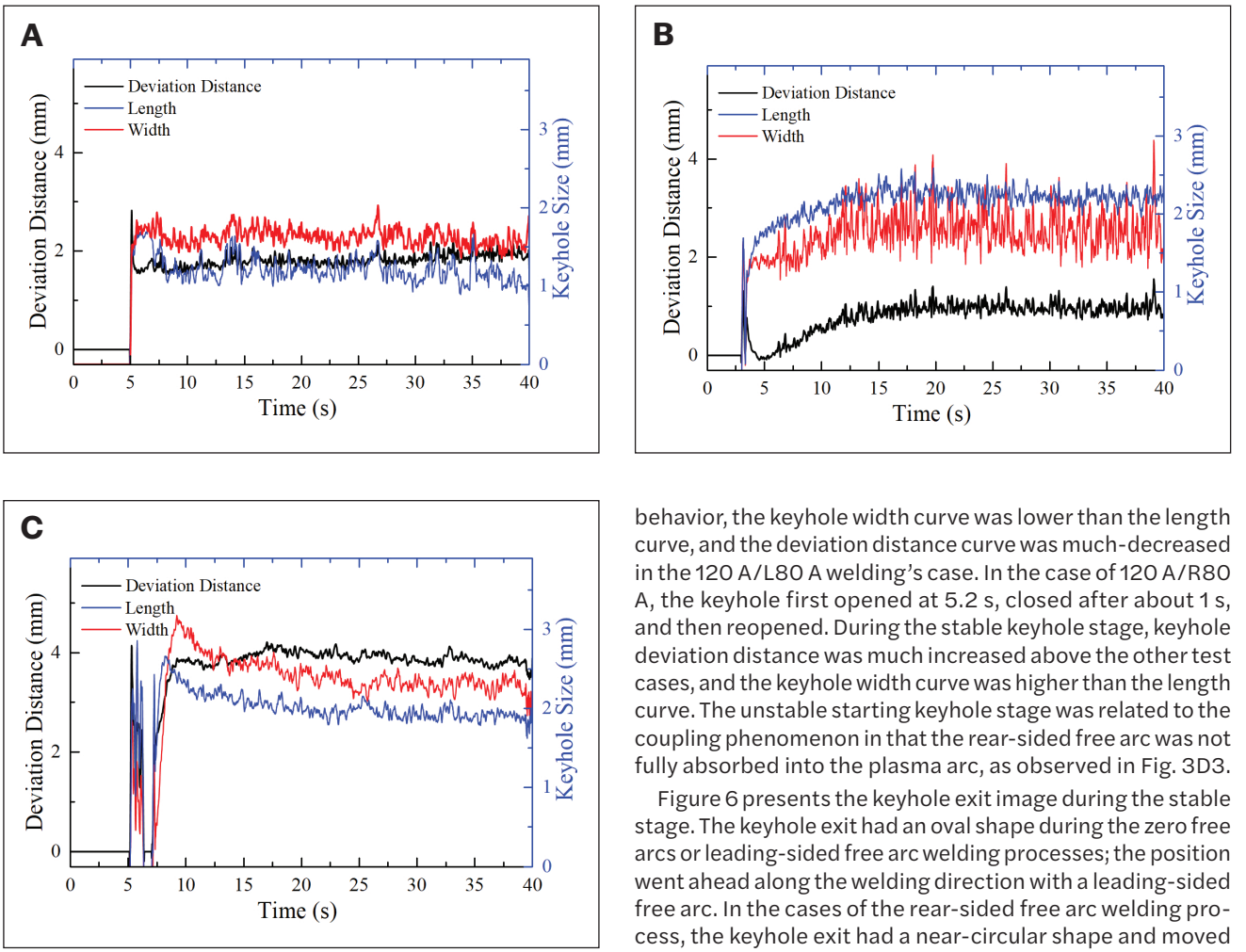

Fig. 5 — Keyhole behavior in welding process: A — 120 A/0 A; B — 120 A/L80 A; C — 120 A/R80 A.

Keyhole Behaviors

The keyhole exits in the welding cases of current I_1 of 120 A were observed by the backside camera. The dimensional and positional parameters (i.e., keyhole length along the welding direction, keyhole width vertical to the welding direction, and the deviation distance (DS) between the keyhole exit center point and the torch axis, as defined in Ref. 25) were calculated from the keyhole exit images. Figure 5 presents the keyhole exit behavior's evolution during the whole welding process. In the case of a single plasma arc at 120 A/0 A, the keyhole opened at 4.94 s with a large deviation distance, and then the deviation distance decreased to the stable stage. During the stable keyhole stage, the keyhole positional and dimensional parameters wavered around their stable values; keyhole width was larger than keyhole length. In the case of 120 A/L80 A, a leading-sided free arc was added into the hybrid arc; the keyhole opened at a shorter period of 3 s, and deviation distance decreased from the peak to 0 levels during the starting stage and then increased to the stable stage. Keyhole dimensional parameters gradually increased during the starting stage and wavered around their stable values. Differing from the single plasma arc welding keyhole behavior, the keyhole width curve was lower than the length curve, and the deviation distance curve was much-decreased in the 120 A/L80 A welding's case. In the case of 120 A/R80 A, the keyhole first opened at 5.2 s, closed after about 1 s, and then reopened. During the stable keyhole stage, keyhole deviation distance was much increased above the other test cases, and the keyhole width curve was higher than the length curve. The unstable starting keyhole stage was related to the coupling phenomenon in that the rear-sided free arc was not fully absorbed into the plasma arc, as observed in Fig. 3D3.

Figure 6 presents the keyhole exit image during the stable stage. The keyhole exit had an oval shape during the zero free arcs or leading-sided free arc welding processes; the position went ahead along the welding direction with a leading-sided free arc. In the cases of the rear-sided free arc welding process, the keyhole exit had a near-circular shape and moved against the welding direction. After camera calibration, keyhole parameters were calculated and are presented in Fig. 6B. The keyhole dimension grew with the free arc current, and keyhole width was not sensitive to free arc position, while keyhole length was larger when the free arc was rear-sided. The deviation distance differed substantially with free arc direction. It grew to 3.5 mm (0.138 in.) at R40 A or even 3.89 mm (0.153 in.) at R80 A from 1.87 mm (0.074 in.) at 0 free arcs, and it decreased to 0.96 mm (0.038 in.) at L40 A or 0.97 mm (0.038) at L80 A. The free arc direction had an obvious influence on the keyhole exit position.

Adding the free arc into the plasma arc increased the heat input into the weld pool. As observed in the arc column, the free arc position influenced the coupling state between the arc and the keyhole, and the melting state in the weld pool should be figured out. The weld end was cut along the middle line to present the melting state in the leading keyhole wall, as shown in Fig. 7. During the keyhole welding process, the powerful arc deposited high-density plasma into the workpiece to heat and melt the solid metal, and the weld pool surface was forced to deform to form a keyhole into the weld pool. If the coupling effect of the heat and pressure was suitable, the keyhole would be fully penetrated and open in the workpiece bottom. If the torch was moving at the welding speed, the melted liquid metal was forced and displaced into the weld pool trailing to the keyhole, the keyhole was in the leading region of the weld pool, and the leading keyhole wall

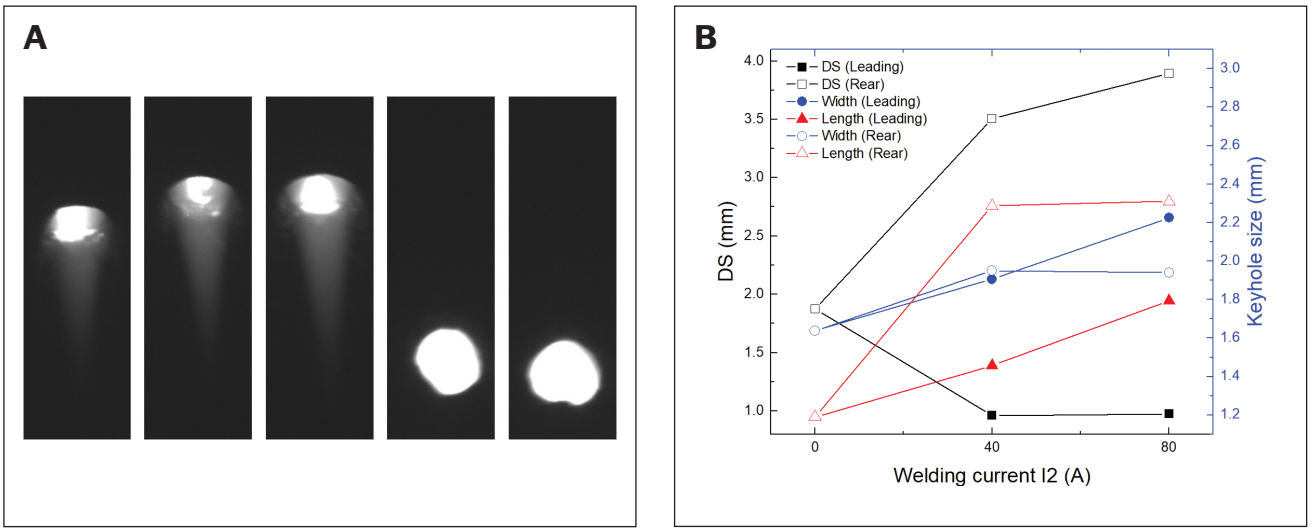

Fig. 6 — Keyhole behavior: A — Stable keyhole image; B — keyhole parameters.

Table 3 — Heat Input (η_1 = 0.65, η2 = 0.4)

Test No.	I_1(A)	U1(V)	I_2(A)	U_2(V)	v(mm/s)	q(J/mm)
3-1-1	118.4	27.7	0	0	3.0	711
3-1-2	118.0	28.1	0	0	3.25	663
3-2-1	118.2	28.4	84.4	9.0	3.0	711
3-2-2	118.5	28.3	84.1	8.5	3.25	663
3-2-3	118.6	28.6	84.4	8.7	3.5	829
3-2-4	118.0	28.5	84.7	9.7	3.75	759
3-3-1	118.3	28.8	85.0	7.0	3.0	714
3-3-2	118.0	28.8	85.3	6.7	3.25	671
3-3-3	117.9	29.0	84.6	7.0	3.5	818
3-3-4	117.9	29.5	84.6	10.2	3.75	750

had little liquid metal, with a thickness of about 10 μm, as presented in weld end sections in Fig. 7. That is, the arc heat was directly deposited into the leading keyhole wall to control the local thermal balance and melting state. Because the heat density in the arc plasma decreased when it traveled along the keyhole channel, the leading keyhole wall was inclined toward the weld pool from top to bottom. The inclined angle is marked in Fig. 7A.

When a leading free arc was added, the plasma arc was attracted to the forward incline, and the leading keyhole wall was observed to be steeper than that obtained in the single plasma arc, while in the rear-sided free arc cases, the leading keyhole wall was increasingly inclined. The inclined angles were measured and are presented in Fig. 7F. The angle was 65.8 deg in the single plasma arc's case, increased to 57.9 deg in the 120 A/L40 A's case and 57.6 deg in the 120 A/L80 A's case, and decreased to 52.1 deg in the 120 A/R40 A's case and 52.3 deg in the 120 A/R80 A's case. The leading keyhole wall inclined degree is the direct reason to determine the keyhole exit deviation distance, as proven in Ref. 26. As observed in the arc images, in the fully penetrated keyhole cases with current I_2 of 120 A, the free arc was fully absorbed into the plasma arc and deposited into the weld pool. That is, equal heat was formed in the weld pool with the same level of free arc current. The difference in the leading keyhole wall angle was highly related to the heat distribution in the hybrid arc.

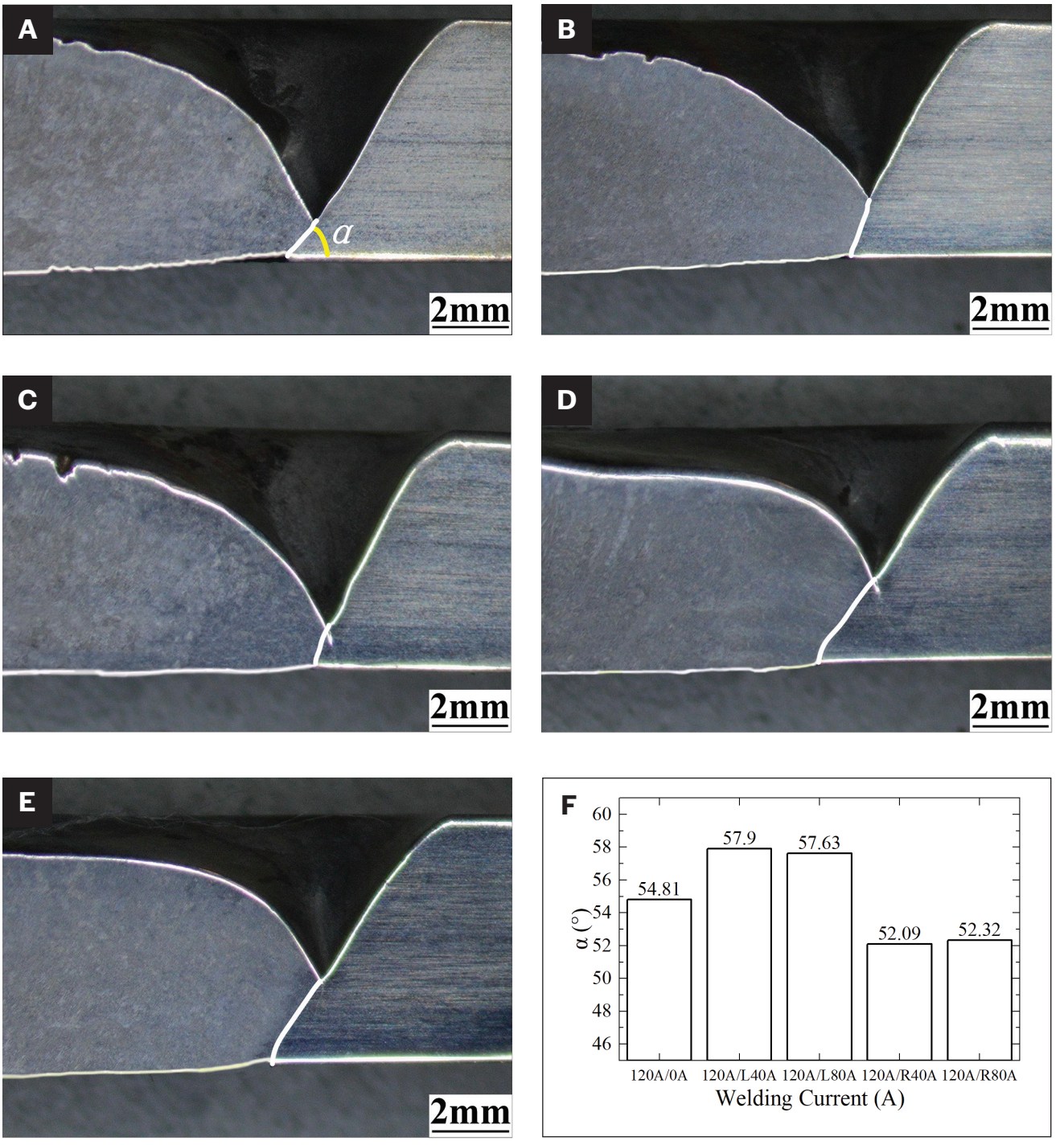

Fig. 7 — Melting state in leading wall: A — 120 A/0 A; B — 120 A/L40 A; C — 120 A/L80 A; D — 120 A/R40 A; E — 120 A/R80 A; F — leading wall angle.

Weld Shape

Cross-sections of the weld in the welding cases of current of 120 A were made and are shown in Fig. 8. In the single plasma arc welding's case, the weld had a narrow melting width. After the free arc was added, the upper half of the weld had a wider melting width. The measured data shows that the melting area in the weld increased from 28.9 mm^2 at the single plasma arc to 32.4 mm^2 at 120 A/L40 A or 32.5 mm^2 at 120 A/R40 A and further to 36.1 mm^2 at 120 A/L80 A or 36 mm^2 at 120 A/R80 A; the front weld width behaved very similarly to the melting area, but the backside weld width did not. This suggests that regardless of the free arc direction, the heat deposited from the added free arc does not transfer into the keyhole bottom but into the upper half of the weld pool. This is good for stabilizing the keyhole weld

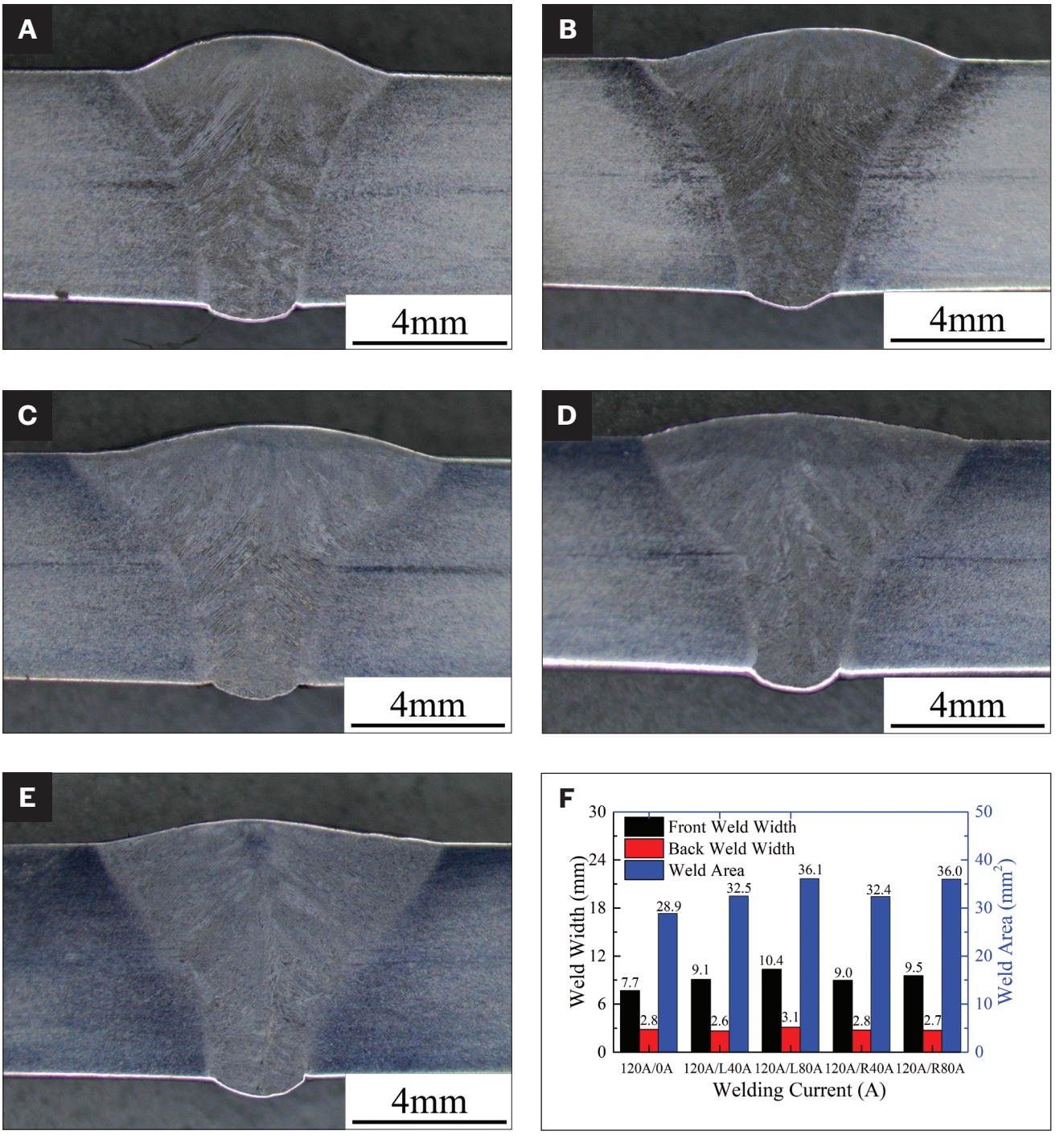

Fig. 8 — Weld cross-section shape: A — 120 A/0 A; B — 120 A/L40 A; C — 120 A/L80 A; D — 120 A/R40 A; E — 120 A/R80 A; F — influence of I_2 to weld width.

pool because the backside weld pool size does not increase, and the surface tension in the backside weld pool surface will not decrease.

Welding Speed

In the hybrid arc process, the added free arc will increase the heat input into the weld pool. To evaluate the influence of the added heat input on the welding speed, Test Group 2 was carried out. A single plasma arc with a current of 120 A was used to figure out the threshold point for a stable open keyhole welding process. At the given current of 120 A, leading-sided or rear-sided free arcs at a current of 80 A were used to test threshold point evolution. As presented in Fig. 9, the max welding speed for stable keyhole welding with the single plasma arc was 3 mm/s for the 120 A/L80 A hybrid arc and the max point increased to 3.5 mm/s, and

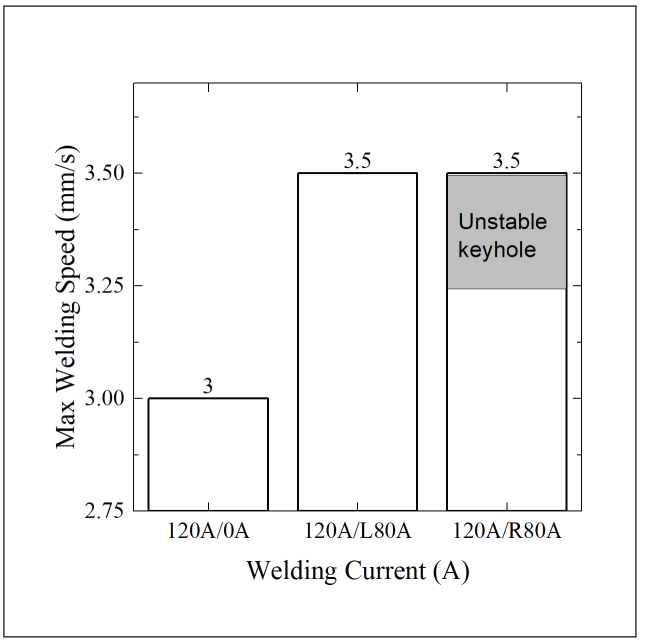

Fig. 9 — Influence of I_2 current on welding speed.

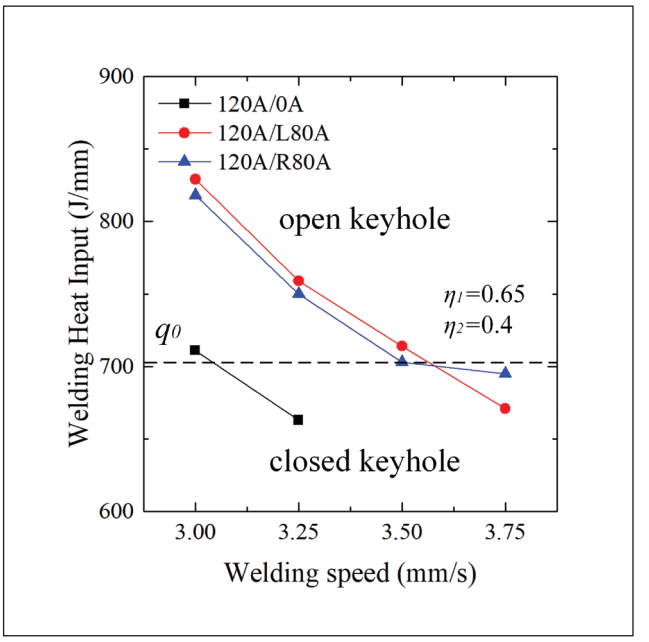

Fig. 10 — Welding heat input estimation.

for the 120 A/R80 A hybrid arc, the max point increased to 3.25 mm (0.128 in.)/s, and unstable keyhole process took place in the range of 3.25~3.5 mm/s. That is, the added heat input helped increase the welding speed for a stable keyhole welding process, while the leading-sided free arc had a better result than the rear-sided case.

Process Efficiency

In the developed hybrid arc, arc pressure was determined by the plasma arc, while the free arc influenced the arc heat output without influencing the arc pressure, as measured in Ref. 17. The welding heat input E was defined as the efficient weld heat input into unit length of weld, following the calculated equation $E=(\eta_1 I_1 U_1 + \eta_2 I_2 U_2)/v$, η, I, U are the efficient factor, welding current and arc voltage of the arc, respectively, and the variables with subscripts 1 and 2 denote the plasma arc and the free arc, respectively. The welding current and voltage were captured in real time during the welding process. The efficient factor η_1 is referred to in Refs. 27 and 28 and was set as 0.65. The weld heat input for the single plasma arc can be easily calculated. The weld heat input threshold point q_0 for a stable keyhole welding process is a point in the range of 663~711 J/mm. The heat input in a hybrid arc should fall into the range to form a stable open keyhole, and we estimate factor η_2 referring to this point. After many traits, $\eta_2 = 0.4$ was chosen as the acceptable value, as shown in Table 3 and Fig. 10.

As shown in Fig. 10, with a single plasma arc or a hybrid arc, the heat input should be higher than the threshold point. After the free arc is absorbed into the plasma arc, the heat input from the free arc increases the heat input into the weld pool and is helpful to get a higher welding speed. As the welding speed increases too high to form enough heat input, the keyhole state turns from open to closed.

Conclusions

1. With a hybrid plasma-free arc, the stable keyhole welding process window is enlarged in aspects of welding current and welding speed, and the hybrid arc with leading-sided tungsten has a more-obvious improving effect.

2. The hybrid arc with the rear-sided tungsten has a smooth front weld surface.

3. The increased heat will enlarge the weld cross-section area but has no obvious influence on the backside weld width; the leading keyhole wall angle increases with a leading-positioned tungsten and decreases with a rear-sided tungsten.

Acknowledgments

The authors are grateful for the financial support for this research from the National Natural Science Foundation of China (51975403).

References

1. Irving, B. 1992. Plasma arc welding takes on the advanced solid rocket motor. *Welding Journal* 71(12): 49–52.

2. Nunes, A. C. 1984. Variable polarity plasma arc welding on the Space Shuttle external tank. *Welding Journal* 63(9): 27–35.

3. Martikainen, J. K., and Moisio, T. J. I. 1993. Investigation of the effect of welding parameters on weld quality of plasma arc keyhole welding of structural steels. *Welding Journal* 72(7): 329s–340s.

4. Steffens, H. D., and Kayer, H. 1972. Automatic control for plasma arc welding with constant keyhole diameter. *Welding Journal* 51(6): 408–418.

5. Zhang, S. B., and Zhang, Y. M. 2001. Efflux plasma charge-based sensing and control of joint penetration during keyhole plasma arc welding. *Welding Journal* 80(2): 157–162.

6. Zhang, Y. M., and Liu, Y. C. 2003. Modeling and control of quasi-keyhole arc welding process. *Control Engineering Practice* 11(12): 1401-11.

7. Zhang, Y. M., and Liu, Y. C. 2007. Control of dynamic keyhole welding process. *Automatica* 43(5): 876-84.

8. Liu, Z. M., Wu, C. S., and Chen, J. 2013. Sensing dynamic keyhole behaviors in controlled-pulse key-holing plasma arc welding. *Welding Journal* 92(12): 381s–389s.

9. Gee, W. F. M., Rybicki, D. J., and Waldron, D. J. 1993. Ternary gas plasma welding torch. United States Patent: No. 5399831.

10. Hessel, L. V. 2014. Increased power density plasma arc welding. Master of Science Thesis, in Technische Universiteit Delft.

11. Li, T. Q., Yang, X. M., Chen, L., Zhang, Y., Lei, Y. C., and Yan, J.C. 2020. Arc behavior and weld formation in gas focusing plasma arc welding. *Science and Technology of Welding and Joining* 25(4): 329–35.

12. Li, T. Q., Chen, L., Zhang, Y., Yang, X. M., and Lei, Y.C. 2020. Metal flow of weld pool and keyhole evolution in gas focusing plasma arc welding. *International Journal of Heat and Mass Transfer* 150(4): 119296.

13. Zhang, Q. L., Fan, C. L., Lin, S. B., and Yang, C. L. 2014. Novel soft variable polarity plasma arc and its influence on keyhole in horizontal welding of aluminum alloys. *Science and Technology of Welding and Joining* 19(6): 493–499.

14. Zhang, Q. L., Yang, C. L., Lin, S. B., and Fan, C. L. 2015. Soft variable polarity plasma arc horizontal welding technology and weld asymmetry. *Science and Technology of Welding and Joining* 20(4): 297–306.

15. Mahrle, A., Rose, S., Schnick, M., Beyer, E., and Füssel, U. 2013. Laser-assisted plasma arc welding of stainless steel. *Journal of Laser Applications* 25(3): 032006.

16. Mahrle, A., Rose, S., Schnick, M., Beyer, E., and Füssel, U. 2013. Stabilisation of plasma welding arcs by low power laser beams. *Science and Technology of Welding and Joining* 18(4): 323–328.

17. Ton, H. 1975. Physical properties of the plasma-MIG welding arc. *Journal of Physics D: Applied Physics* (8): 922–933.

18. Asai, S., Ogawa, T., Ishizaki, Y., Minemura, T., Minami, H., and Miyazaki, S. 2012. Application of plasma MIG hybrid welding to dissimilar joints between copper and steel. *Welding in the World* 56(2): 37–42.

19. Wang, L., Zhang, C., and Wu, C. S. 2020. Experimental study on controlled pulse keyholing plasma arc welding assisted by ultrasonic vibration. *The International Journal of Advanced Manufacturing Technology* 107(11): 4995-5009.

20. Wang, L., Chen, J., and Wu, C. S. 2021. Auxiliary energy-assisted arc welding processes and their modelling, sensing and control. *Science and Technology of Welding and Joining* 26(5): 389-411.

21. Qiu J. Y., and Liu, Z. M. 2021. Hybrid a free arc into constraint-arc to improve arc pressure control behavior. *Journal of Manufacturing Processes* 64(7): 766–773.

22. Li, K. H., and Zhang Y.M. 2008. Consumable Double-Electrode GMAW Part II: Monitoring, Modeling, and Control. *Welding Journal* 87(2): 44-s–50-s.

23. Chen, J. S., Lu, Y., Li, X. R., and Zhang Y. M. 2012. Gas Tungsten Arc Welding Using an Arcing Wire. *Welding Journal* 91(10): 261-s–269-s.

24. Liu, Z. M., Wu, C. S., and Gao, J.Q. 2013. Vision-based observation of keyhole geometry in plasma arc welding. *International Journal of Thermal Sciences* 63(1): 38–45.

25. Liu, Z. M., Wu, C. S., and Chen, M. A. 2014. Experimental sensing of the keyhole exit deviation from the torch axis in plasma arc welding. *The International Journal of Advanced Manufacturing Technology* 71(3): 1209–1219.

26. Liu, Z. M., Wu, C. S., Cui, S. L., and Luo, Z. 2017. Correlation of keyhole exit deviation distance and weld pool thermo-state in plasma arc welding process. *International Journal of Heat and Mass Transfer* 104(1): 310–317.

27. Fuerschbach, P. W., and Knorovsky, G. A. 1991. A study of melting efficiency in plasma arc and gas tungsten arc welding. *Welding Journal* 70(11): 287–297.

28. Wilkinson, J. B., and Milner, D. R. 1960. Heat transfer from arcs. *Welding Journal* 7(2): 115–128.

ZUMING LIU *(zuming.liu@tju.edu.cn)*, **FEI LIU**, and **JIAYU QIU** are with the School of Materials Science and Engineering & Tianjin Key Laboratory of Advanced Joining Technology, Tianjin University, Tianjin, China.